# Optical and structural properties of CdS:$Pb^{2+}$ nanocrystals

R. Gutiérrez[a,*], O. Portillo[a], M. Chávez[b], H. Juárez[b], M. Pacio[b], L. Chaltel[a],
M. Zamora[a], M. Lazcano[a], E. Rubio[c], and G. Hernandez[a]
[a]*Materials Science Laboratory, Facultad de Ciencias Químicas, Universidad Autónoma de Puebla, P.O. Box 1067, Puebla, Pue., 72001 México.*
[*] *Tel. (01 222) 2-29-55-00 Ext. 7519.*
*e-mail: osporti@yahoo.mx*
[b]*CIDS-ICUAP, Universidad Autónoma de Puebla, Puebla, Pue., 72001 México.*
[c]*Centro Universitario de Vinculación y Transferencia Tecnológica, Universidad Autónoma de Puebla, Ciudad Universitaria, Colonia San Manuel, Puebla, Pue., 72001 México.*

Received 8 April 2015; accepted 29 May 2015

The goal of this work is to study the effects of doping on structural, morphological and optical properties of CdS thin films as a function of $Pb^{2+}$ concentration. Thus, nanoparticles were synthesized by chemical bath and a thickness decrease of ∼575-200 nm range was observed. In Fourier-transform infrared spectroscopy, all the samples showed a sharp stretching mode observed at ∼1384 $cm^{-1}$ corresponding to the vibration mode of $CO_3^{-2}$. X-ray diffraction studies show that the size of crystallites is in the ∼33-12 nm range. The peaks belonging to primary phase are identified at the $2\theta = 26.5^\circ$ and $2\theta = 26.00^\circ$, corresponding to CdS and PbS respectively. Thus, a shift in maximum intensity peak from $2\theta = 26.4^\circ$ to $28.2^\circ$ is observed. Likewise peaks at $2\theta = 13.57^\circ$, $15.91^\circ$ correspond to lead perchlorate thiourea. The optical, absorption, and transmission properties of the films were determined by UV-vis spectrophotometry, optical energy gap was found to range from 2.1 to 2.4 eV. Raman spectroscopy on doped films showed a shifting of these modes that can be attributed to strain, stress effects, defects, phonon confinement, and variation in phonon relaxation with grain size.

*Keywords:* Chemical bath; CdS; cell potential; nanoparticles; coordination complex; doping.

PACS: 71.20.Nr; 68.55.A; 64.70.kg

## 1. Introduction

Ternary II-IV-VI compounds in the form of thin films have attracted an ever-increasing attention due to their potentials applications in integrated optics and photovoltaic devices. Thin films of CdS and PbS are promising photovoltaic materials as their variable band gap ($E_g$) could be adjusted to match the ideal $E_g$ (1.6 eV) required for achieving a most efficient solar cell. PbS is a semiconductor material belonging to IV-VI group with a direct $E_g$ = 0.4 eV suitable for infrared detection applications [1,2]. It has also been used as photoresistance, laser diode, humidity and temperature sensors [3]. On the other hand, doping CdS films incorporating various elements have already been studied given that the structural and optical properties of CdS are strongly modified, and such effect of doping is under steadfast investigation to tune the properties of interest. Recent advances in CdS-based materials research are established by growing Fe, [4] Ga, [5] Pb, [6] Zn, [7] B, [8] etc., doped CdS thin films and nanostructures. As CdS and PbS are highly sensitive to light and in view of their practical applications, a study of their mixed thin films structure as electrochemical converters is of technical importance. Mixing of CdS and PbS would be expected to be interesting because (a) both are very good photoconductors, (b) it is showed both direct and indirect $E_g$. In this study we investigate structural and optical properties of $Pb^{2+}$ -doped CdS thin films prepared by chemical bath (CB). The thickness of layers was in the ∼625-200±10 nm range, as determined by utilising a Dektak II profilometer.

## 2. Chemical reactions

The reaction mechanism for forming CdS, Pb-doped CdS Dissotiation in alkaline medium of $Pb(CH_3OO)_2$ induces the formation of $Pb_{2+}$ and $CH_3OO$ ion, according to:

$$Pb(COOCH_3)_2 \Leftrightarrow Pb^{2+} + 2CH_3COO^- \quad (1)$$

and

$$Cd^{2+} + 2OH^- \Leftrightarrow Cd(OH)_2$$
$$\Delta G^0 = +82.44 \text{ kJ/mol} \quad (2)$$
$$Pb^{2+} + 2OH^- \Leftrightarrow Pb(OH)_2$$
$$\Delta G^0 = +63.22 \text{ kJ/mol} \quad (3)$$

$Cd(OH)_2$ and $Pb(OH)_2$ solutions start precipitating when $k_{sp}$ is exceeded, $Cd(OH)_2$: $k_{sp} = 2 \times 10^{-14}$ mol/L, and $Pb(OH)_2$: $k_{sp} = 4.0 \times 10^{-15}$ mol/L in water at 25°C [9]. The $Cd(OH)_2$ and $Pb(OH)_2$ precipitate dissolves when the $NH_4NO_3$ is added to the solution to form the $[Cd(NH_3)_4]^{2+}$ complex ion, with stability constants of complexes of $[Cd(NH_3)_4]^{2+}$ = 16.24 and $[Pb(NH_3)_4]^{2+}$ = 15.59 respectively [10]. Finally,

the CdS or PbS thin films formation takes place, then

$$[Cd(NH_3)_4]^{2+} + S^{2-} \Leftrightarrow CdS + 3NH_4^+ + 3e$$
$$\Delta G^0 = +163.02 \text{ kJ/mol} \quad (4)$$
$$[Pb(NH_3)_4]^{2+} + S^{2-} \Leftrightarrow PbS + 3NH_4^+ + 3e$$
$$\Delta G^0 = +502.96 \text{ kJ/mol} \quad (5)$$

$k_{sp}$ of CdS: $k_{sp} = [Cd^{2+}][S^{2-}] = 8 \times 10^{-28}$ mol/L and PbS: $k_{sp} = [Pb^{2+}][S^{2-}] = 10^{-27}$ mol/L [9], are very close, thereby formation of CdS and PbS can occur simultaneously [11] and starts precipitating when $k_{sp} = [OH^-][Pb^{2+}]$ is exceeded. In a general, we have:

$$[Cd(NH_3)_4]^{2+} + S^{2-} + [(NH_3)_4]^{2+} \Leftrightarrow CdSPb^{2+} + 8NH_{3(g)} \uparrow$$
$$\Delta G^0 = -139.64 \text{ kJ/mol} \quad (6)$$

Based on the Gibbs free energy obtained from the and PbS is as following with thiourea hydrolysis $SC(NH_2)_2$ leading to the formation of $S^{2-}$ and $CO_3^{2-}$ ions equilibrium analysis, the $Pb^{2+}$ ionization state is probably present in the volume of CdS under our working conditions. If

$$2SC(NH_2)_2 + 80H^- \Leftrightarrow 2CO_3^{2-} + 4NH_3 + 2H_2O \quad (7)$$

$\Delta G^0 < 0$, the reactions (7) are spontaneous. It immediately appears that the reaction can take place either in the bulk of the solution (homogeneous precipitation process) or at the substrate surface (heterogeneous process), the second one leading to the film formation from two distinct mechanisms. The first one is a growth mechanism involving the reaction of atomic species at the surface and corresponds to an atom-by-atom process, also called ion-ion process [12]. The predominance of one given mechanism is governed by classical laws of homogeneous nucleation on a solid surface, involving the saturation ratio in the solution and the catalytic activity of the substrate. For chalcogenide semiconductors, the crystal size has been shown to be dependent on the deposition mechanism: the cluster mechanism results in smaller crystal size than the ion-ion mechanism [13]. In the cluster mechanism, the size of the metal hydroxide colloids present in the deposition solution is expected to define the product crystal size, and this size will depend largely on doping [14].

### 2.1. Experimental section

#### *2.1.1. Preparation of the doped and undoped CdS films*

Preparation of polycrystalline CdS thin films on glass substrates, both undoped (CdS0-PbS0) and doped (CdSPb) where volume-solution $V_{[Pb^{2+}]}$ containing the doping $Pb^{2+}$ chemical agent were grown by chemical bath (CB). The substrates of commercial quality microscopic glass slide of dimensions $24 \times 75$ mm were previously degreased in acid-chromium ($K_2Cr_2O_7$/HCl/$H_2O$) mixture for 24 h and then rinsed in deionized water and finally dried in a clean hot-air flow. The substrates were then immersed in solution. CdS films with seven different levels of doping ($V_{[Pb^{2+}]}$) were obtained by the addition in situ of: 4, 6, 10, 14, 20, 25, 30 mLs in the solutions for CdS growth, with the bath containing the solutions of: CdCl2 (0.02 M), KOH (0.1 M), $NH_4NO_3$ (1.2 M), $SC(NH_2)_2$ (0.1 M). These solutions are routinely added to the reaction mixture during the growth of the CdS0 films. The solutions were mixed and the final solution kept at $90 \pm 2°$C, while the substrate remains inside the solution. The optimal doping concentration ($V_{[Pb^{2+}]}$) $Pb(CH_3CO_2)_2$ (0.05 M) was determined after several trials, when the films had attained good adherence. All the solutions used were prepared with deionized water with a resistivity of 18.2 MΩ. The samples were labeled as PbS0-CdS0 for the undoped sample and CdSPb4,...,CdSPb30 (CdS:Pb) for the doped samples. The total volume of the growing-solution consisted of the volume-solution ($V_{CdS0}$) for the CdS0 growth plus the volume-solution: $V_{CdS} + V_{[Pb^{2+}]} = V_{tot}$ For the first 5 min of reaction time, the solution remained transparent, indicating the occurrence of decomposition reaction. Beyond 10 min, the solution appears in green colour, and at the final stage turned dark gray, indicating the formation of doped- $Pb^{+2}$ CdS films (CdS:Pb). After completion of the deposition time (45 min), samples were removed from the solution, rinsed ultrasonically in hot deionized water for 5 min, and dried in air. Details of preparation of polycrystalline PbS0 by CB method has been previously reported, using $Pb(CH_3CO_3)_2$ (0.01 M), KOH (0.5 M), $NH_4NO_3$ (1.5 M), $SC(NH_2)_2$ (0.2 M) solutions [14,15].

### 2.2. Characterization

The surface morphology of the films was done using a scanning electron microscope (SEM) JEOL Model JSM6490. The compositional analysis was carried out using energy dispersive X-ray spectroscopy (EDS). The Fourier transform infrared spectroscopy (FT-IR) spectrum was recorded using a Perkin Elmer spectrophotometer in the 400-4000 $cm^{-1}$ wavelength region. The X-ray diffraction (XRD) patterns of the solid samples were acquired in a D8 Bruker Discover Series 2 Diffractometer with Cu K$\alpha$ radiation of wavelength $\lambda = 1.5408$ Å. The grain size was determined by utilizing the Scherer's formula on XRD patterns. The optical absorption studies were carried out using UV-Vis-IR spectrophometer (Cary-5000) in the 300-900 nm wavelength range at room temperature. Raman spectra (RS) were excited with the 600 line of an $Ar^+$ ion laser and recorded with a Dilor XY triple monochromator equipped with a Peltier-cooled CCD detector.

## 3. Results and discussion

Figure 1 shows the images of the CdS0-CdS:Pb- PbS0 thin films, and it is worth-interesting to note the color change. The

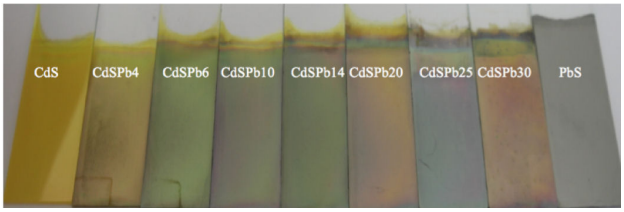


FIGURE 1. Photography of CdS0-CdSPb-PbS0 thin films.

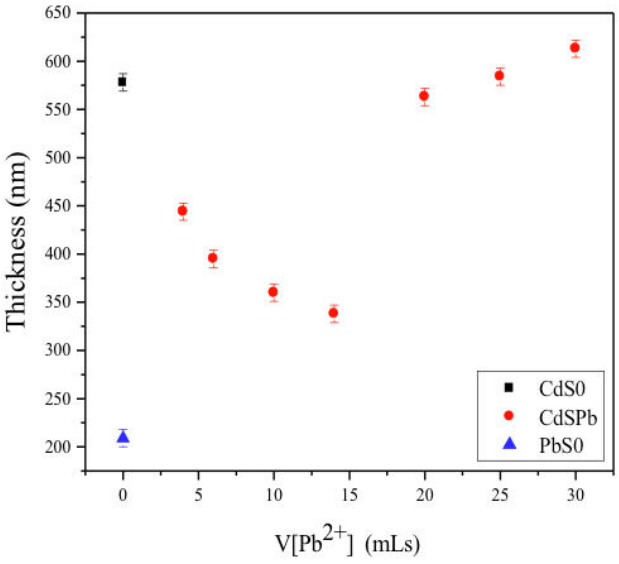


FIGURE 2. Thickness vs. $V_{[Pb^{2+}]}$ CdS0-CdSPb-PbS0 thin films.

CdS0 films look yellowish and CdSPb4 to CdSPb30 samples look pale-green-yellow-dark-brown and PbS0 metallic-dark.

Figure 2 shows the thicknesses vs. $V_{[Pb^{2+}]}$ of CdS0-CdS:PbPbS0 thin films. Measurements of thickness decrease of ∼575-200 nm range for CdSPb4 to CdSPb10 as total thickness of the films growth. The highest thickness obtained was in the case CdSPb30 of ∼625 nm. Two different regions can be observed, a first region were the films decrease approximately linearly with an increase of $V_{[Pb^{2+}]}$, indicating constant growth, and a second region, whereas films growth reaches saturation and increases with $V_{[Pb^{2+}]}$. The same behavior while varying temperature is also observed for other semiconductors such as ZnS [16] and MnS [17], having explained this phenomenon by considering two competing processes taking place in deposition bath: one process includes the heterogeneous and homogeneous precipitation of CdS, which leads to the film growth; the other ones involves the dissolution of the pre-formed CdS films, which result in a decrease of the films thickness. In the initial time of deposition, the source materials are sufficient; the process of heterogeneous and homogeneous precipitation play a more important role than the dissolution process leading to an increase in film thickness [18]. This can be explained by different values of stability constant of $Cd^{2+}$ and $Pb^{2+}$ complexes [10]. The differences in the nature of layers growth of CdS0-CdS:Pb-PbS0 films can be explained by the process stages. When the doping is applied to the solution and heated, $[(NH_3)_4]^{2+}$ ($k_f = 1.3 \times 10^7$) and $[(NH_3)_4]^{2+}$ ($k_f = 2.0 \times 10^{35}$) complexes start to orient on active centers of the substrate surface forming CdS:Pb growth centers.

Films deposited with ammonia or hydrazine solution result in thinner films while films free of these compounds result in thicker films. This effect is due to low complexation of $Pb^{2+}$ ions. At a low deposition rate, concentration of free $Pb^{2+}$ ions is lower due to high complexation resulting in thinner films, but concentration of free $S^{2-}$ ions is higher. Typically, chemically chalcogenide films by CB are formed from the reaction between a metallic salt and thiourea in a ammonia alcaline solution [19]. The results obtained in this work show an almost linear dependence in decrease of thin film thickness with the increases of doping CdSPb4 to CdSPb10 samples. From films CdSPb15-CdSPb30, the increase of thin film thickness is a result of the increase doping. The dependence of film thickness of deposition was complicated, but also had a character close to linear. The maximum possible number of growth centers is determined by the number of active centers on the substrate surface, which is considerably less than the reactive particles in solution. Under the influence of continuous doping solution flow, the growth centers increases and turn into layer. This fact slows the increase of films thickness, and at the same time alter the film weight grain. In CB technique, the film growth starts initially with an incubation period, where no clearly observable growth occurs. The period corresponds to the nucleation step followed by a subsequente linear growth [20]. The compositional analysis was carried out using energy dispersive X-ray spectroscopy (EDS), the values listed in Table I are not so far from the true atomic concentration. In Table I are compiled the atomic concentration of Cd, S and Pb. It can be appreciated the increase in concentration of Pb, reaching percent values of up to 4.36%.

The surface morphology of the CdS0-CdSPb-PbS0 thin films was studied by scanning electron microscope (SEM). Figure 4 shows SEM micrograph of (a) CdS0 film, (b) CdSPb30 and (c) PbS0, respectively. Microstructures of doped samples (CdS:Pb) exhibit appreciable changes as compared to that of undoped (CdS0) sample and these changes can be attributed to a change in ionic fraction of a compound on

TABLE I. Cd, S, and Pb concentration in CdS0-PbSPb-PbS0 samples for $V_{[Pb^{2+}]}$ values studied measured of electron dispersion spectroscopy (EDS).

| Sample | Atomic concentration (%) | | |
|---|---|---|---|
| | Cd | S | Pb |
| CdS0 | 49.10 | 50.90 | 0 |
| CdSPb6 | 47.55 | 52.28 0.17 | |
| CdSPb14 | 47.96 | 49.86 2.18 | |
| CdSPb20 | 47.00 | 49.33 | 3.67 |
| CdSPb30 | 47.80 | 47.84 | 4.36 |
| PbS0 | 0 | 48.9 | 51.1 |

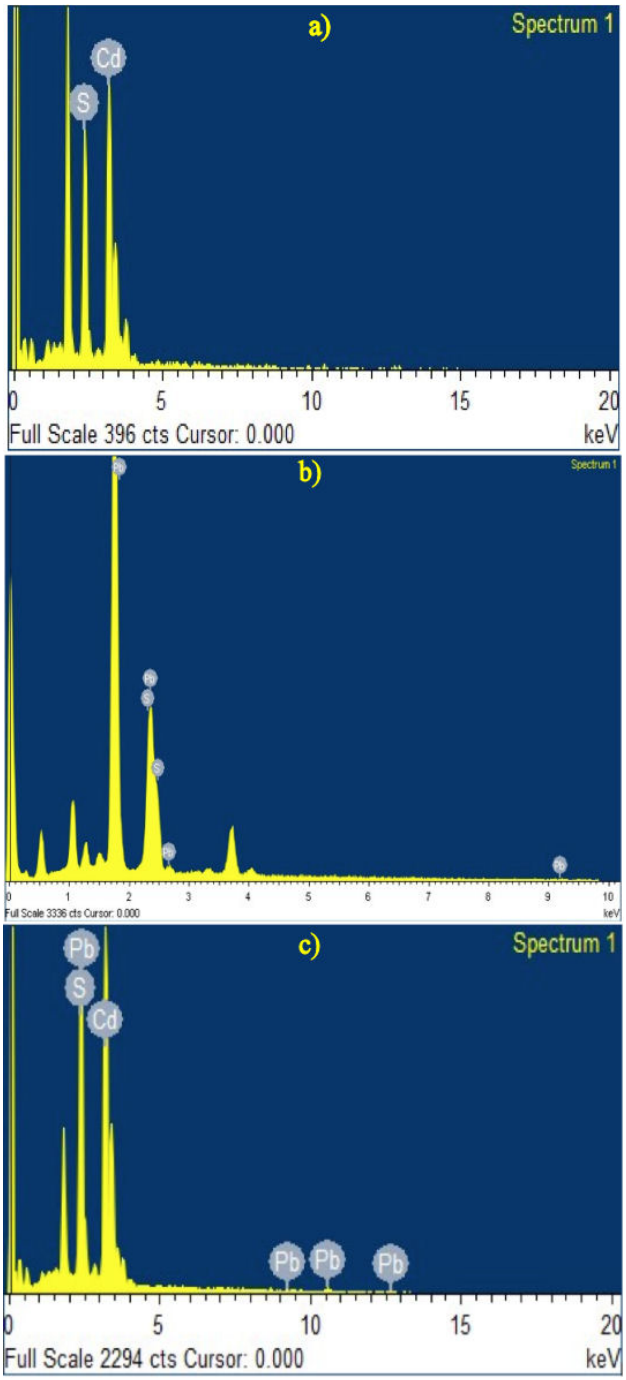


FIGURE 3. EDS spectra of (a) CdS0, (b) CdSPb30 (c) PbS thin films.

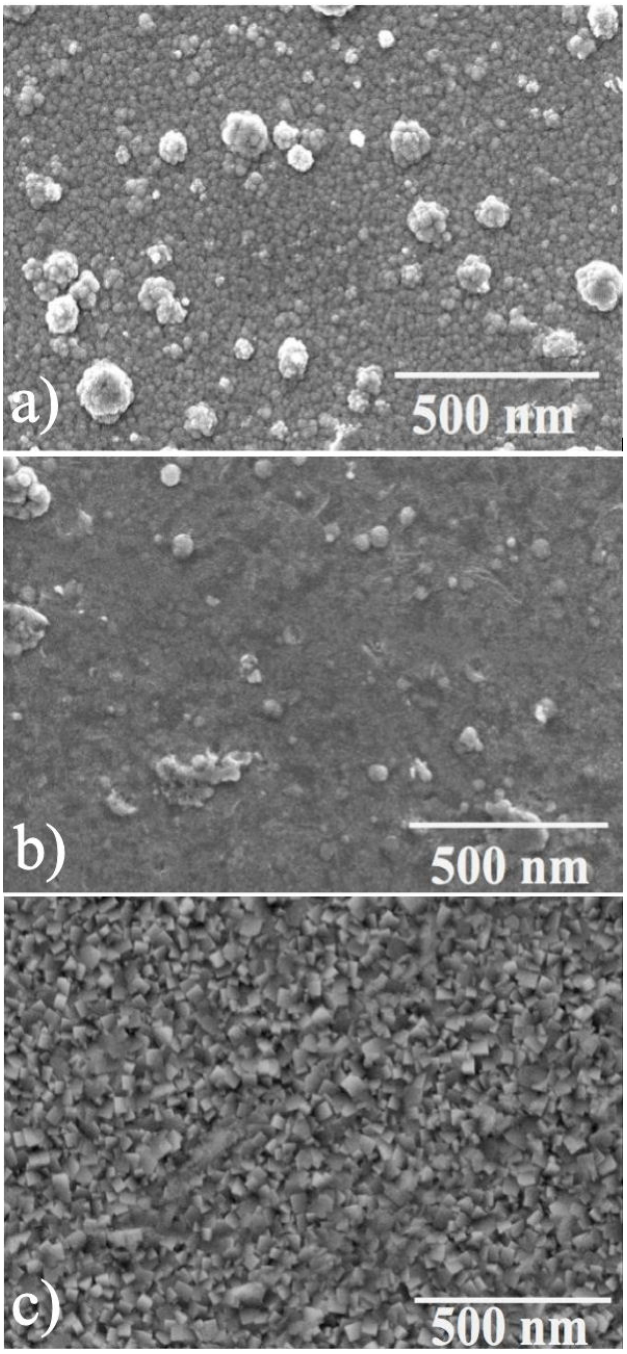


FIGURE 4. SEM micrograph of (a) CdS0, (b) CdS30 and (c) PbS0 respectively.

on doping. This result correlates with the improvement in crystallinity with increasing $V_{[Pb^{2+}]}$ as evident from structural studies. It can be seen images from (a) displayed a continuous and compact polycrystalline films with well-defined grain boundaries. As clearly seen in Fig. 3 (c), large isolated clusters formed on surface of the PbS0 films. The grain size (GS) were estimated in the 10-30 nm range. Two different phenomena explain the formation of these aggregates. First, the formation of aggregates in the chemical solution by doping is related to nucleation around $Pb^{2+}$ ion on the substrate surface. Second, there are two growth mechanism for CB, namely, ion-ion and cluster-bycluster mechanisms. In CB, these two mechanisms occur randomly and the aggregates form in the cluster-cluster mechanism.

Figure 5 shows the Fourier transform infrared (FT-IR) spectra of CdS0-CdS:Pb-PbS0 nanoparticles. When the CdS0 film is loaded with $V_{[Pb^{2+}]}$, the FT-IR spectra changed with respect to pure CdS0 films. The absorption bands observed in the 2800-3000 $cm^{-1}$ region are attributed to the vibration of $-CH_2$ groups and the other two bands located in

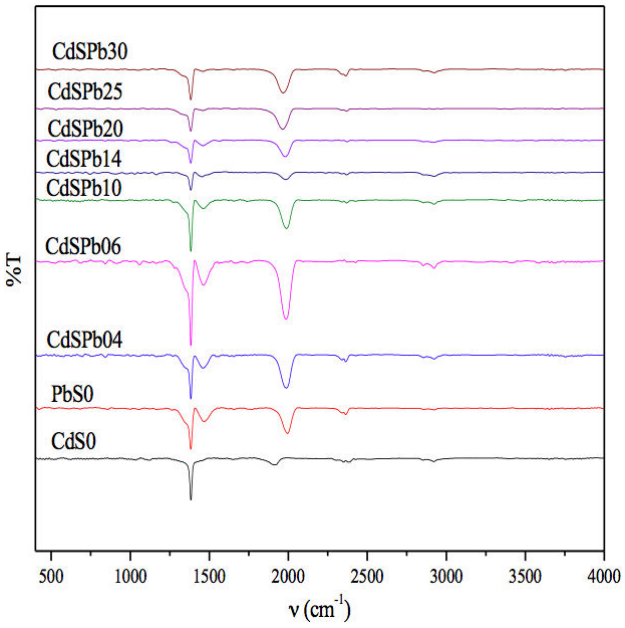


FIGURE 5. FTIR spectra of CdS0-CdSPb-PbS0 nanoparticles.

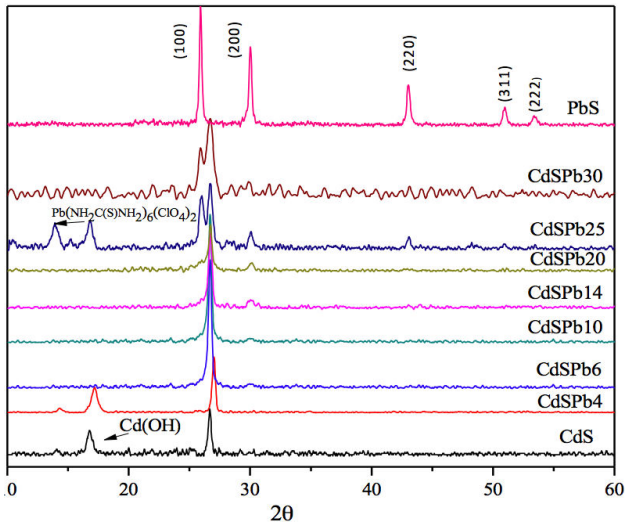


FIGURE 6. XRD diffraction patterns for CdS0-CdS-Pb-PbS0 films.

in the 1725-1690 and 1440-1395 cm$^{-1}$ region are indexed to vibrations modes of C=O and OH$^-$ groups [21]. All the samples showed a sharp stretching mode observed at 1384 cm$^{-1}$ corresponding to the vibration mode of $CO_3^{2-}$, (see Eq. (1), (4), and (5)). The bands around 1406 cm$^{-1}$ are the signal of -CN bonding (due to $CS(NH_2)_2$ by-products), while the peaks at ∼686 cm$^{-1}$ are referred to be particular peaks of the -SC bond [22]. The main spectral features are similar, except the intensity of ∼1384 cm $^{-1}$ absorption bands. The low intensity bands observed for -COO-H bonds in induced CdS:Pb samples is in conformity with the reaction (2). PbS0-CdSPb30 samples show bands located at ∼1586 cm$^{-1}$ that can be attributed to the characteristic bands of the ($CH_3COO^-$) carboxylate groups, corresponding to the -$CH_2$ bending mode and asymmetric and symmetric C-O stretching modes of the -$COO^{-1}$ groups respectively, which would correspond to adsorbed organic species from solution (acetate ion and hydrolysis by-products), attributed to the dissociation of $Pb(COOCH_3)_2$ [23]. However, the stretching vibration of S-H bond (∼2560 cm$^{-1}$) are not observed in Fig. 3 indicating that $Pb(COOCH_3)_2$ films combines on surface of the CdS:Pb with concomitant loss of the S-H bonds [24]. The absence of S-H stretching bands around ∼2560 cm$^{-1}$ indicates that is bound to surface lead through Pb-S chemical bonds by cleaving its hydrogen bonds. The Pb-S bonds are mainly electrovalent bonds; the FTIR of PbS does not show strong bands associated with Pb-S stretching and bending vibration for such bond. Absorption band occurring at ∼619 cm$^{-1}$ are due to Cd-S stretching vibration [24] but this was absent here. When $V_{[Pb^{2+}]}$ is added and PbS0 are supplied into crystals, the interactions reduce as some of the PbS will react to forms nanoparticles. A comparison of these spectra showed clearly that many carboxylate and $CO_3^{2-}$ groups remain on the surface of nanocrystals even after excessive washing. After deposition, CdS0-CdS:PbPbS0 layers were thermally pre-treated in vacuum for removing of residual water at 100°C for 10 min.

Figure 6 shows the XRD diffraction patterns for CdS0CdS:Pb-PbS0 samples. CdS exists in two crystalline modifications: the Wurtzite (WZ) 25 and zinc blende (ZB) phase [26]. As can be seen, the obtained diffraction pattern for CdSPb4 sample shows a predominant peak at $2\theta = 26.5°$ which can be assigned to (111) plane of ZB CdS phase. Moreover, the intensity of peak at $2\theta = 28.2°$ is due to diffraction from the (101) plane WZ phase whereas at $2\theta = 26.4°$ position can be co-occupied by the (111) plane of ZB phase as well as the (002) plane WZ. However, the maximums peak intensity for both phases are different, *i.e.*, ZB maximizes at: $2\theta = 26.4°$ corresponding to the (111) plane, whereas WZ phase has its maximum intensity peak at $2\theta = 28.2°$ corresponding to (101) plane [27]. Formation of the WZ phase is likely, at least to large extent, because the characteristic diffraction peak from the (002) planes of the structure was completely absent when the CdS0 film was deposited. The shift in the diffraction angles are due to the incorporation of $Pb^{2+}$ at the sub-lattices sites of $Cd^{2+}$. It has been reported in the literature that the probability that CdS dissolves in the PbS lattice at room temperature is very low [28]. In this case of extremely small particles, where the contribution of surface free energy is very important, some deviations cannot be excluded. In CdS0 and CdSPb4 samples, a cadmium hydroxide [$Cd(OH)_2$] film is clearly seen to have been deposited. The formation of $Cd(OH)_2$ preceding a CdS deposition can be explained by the fact that cadmium ions are labile in aqueous media and equilibrium are rapidly stabilized in solution [29]. The concentration of sulfide ions is limited by the thiourea decomposition and the decomposition of the weak acid is $H_2S$, $k_a = 9.1 \times 10^{-8}$. The activation energy for the films growth has been found as 56.7 kJ/mol, and this is close to the value for the hydrolysis of thiourea,

which was used as sulphur source in CB. It was therefore supposed that the rates of both the films growth and precipitation are limited by that of the hydrolysis of thiourea in the alkaline medium [30]. These diffraction peaks become sharper for CdSPb4, CdSPb6 and CdSPb14. From XRD patterns it can be assured that the $Pb^{2+}$ forms PbS according to the peak located at $2\theta \sim 30°$ in CdSPb14 to CdSPb30 samples. However, CdSPb6 sample shows a peak at $2\theta \sim 26.5°$ indicating a preferred orientation. From the XRD study we can infer that the formation of the CdS:Pb occurs in the early stage, following by the formation of PbS0 nanocrystallites in the stage of the film growth, although the formation of films from the bath in absence of acetic is also observed [30]. It is found in this study that the reaction leads to formation of nanocrystalline CdS:PbS films together with a slight decrease in the size of crystallites. These peaks do no match exactly with the reported plane spacing for ZB and WZ phases, and this can be explained by the broadening of peaks from CdSPb25 and CdSPb30, which can be due to the small size of the crystals and by presence of strains that possess multiple facet diffraction peaks, which is the result of multidirectional growth of the synthetized nanocrystals. The peaks belonging to primary phase are identified at $2\theta = 26.5°$ and $2\theta = 26.00°$ corresponding to CdS0 and PbS0 respectively. Thus, a shift in maximum intensity peak from $2\theta = 28.2°$ to 26.4° is clear indication of possible transformation of ZB phase to WZ phase. It is worth-noting the values of electronegativity for Pb (2.33) and Cd (1.69), which are favourable to form a solid solution [31]. However in the CdSPb25 film, peaks located angular positions: $2\theta = 13.57°$ and 15.9° correspond to $[Pb(NH_2(S)C(NH_2)_2)_2](ClO_2)_2$, lead perchlorate thiourea, according to standard (JDDC 0531447). In the alkaline medium CB, the atom-atom growth of CdS is supposed to proceed by decomposition of adsorbed thiourea-hidroxocadmium complex as expressed by [13]

$$[Cd(OH)_2SC(NH_2)_2]_{ads} \Leftrightarrow CdS + CO_3^{2-} + OH^- + 2NH_3 + 2H_2O + 2e \qquad (8)$$

In our opinion, this result indirectly proves the mechanism proposed by Ortega-Borges and Lincot [32]. In this mechanism the rate-determining step is the decomposition of the metastable complex for which activation energy values are close to those calculated that can be expected. On the basis of the above CdS0 precipitation mechanism, the high $V_{[Pb^{2+}]}$. can assure that the CdS0 large cluster may not cause a non-uniform thin film to CdS:Pb growth. Therefore the more metastable complex can acquire enough activation energy to decompose and to precipitate the crystalline CdS0 film due to high $V_{[Pb^{2+}]}$. It should be noticed that it not only generates CdSPb and $Cl^-$ ion but it is also generated the $ClO_4^-$ anion in our system, and the coproduced $ClO_4^-$ is oxidized by reduction. In this $V_{[Pb^{2+}]}$, a $Cl^-$ ion is oxidized by the $NO_3^-$ in the system, affording the coproduced $ClO_4^-$ according to:

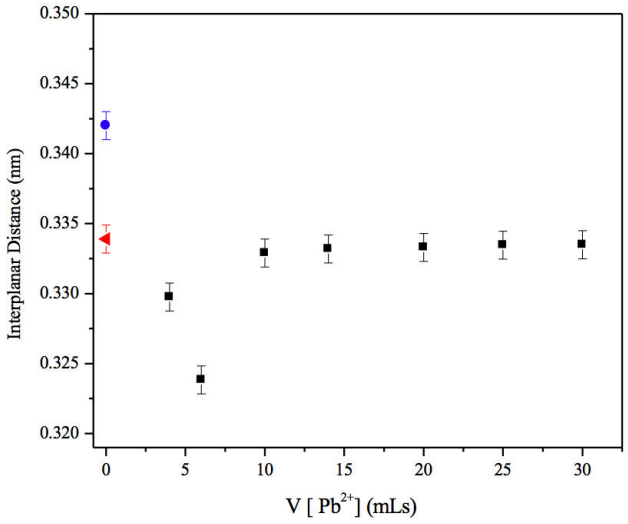


FIGURE 7. Interplanar Distance (111) for WZ phases Hexagonal and Cubic (ZB) CdS0-CdSPb-PbS0 samples.

$$3H_2O + Cl^- + NO_3^- \Leftrightarrow ClO_4^+ + NH_4 + 2OH^- \qquad (9)$$

PbS0 diffractogram display peaks located at the following angular positions: $2\theta = 26.00°$, 30.07°, 43.10°, 51.00°, 53.48°. They are related to the (111), (200), (220), (311), (222) reflection planes for the ZB phase of the PbS0 respectively. All the diffraction peaks for PbS0 can be perfectly matched to the reference patterns (JCPDS 05-0592) displaying the ZB crystalline phase [15].

Figure 7 displays the (111) interplanar distance (ID) for ZB phase, calculated from the $2\theta$ peak position, vs $V_{[Pb^{2+}]}$: this ID, in practice, coincide with (111) ID of the ZB phase. The CdS WZ structure was reported to give rise generally to three interplanar spacing of 3.34 Å, 2.05 and 1.75 Å, while 3.11 Å, 2.67 Å, 1.85 ÅID can be ascribed to ZB structure. It can be appreciated that ID first decreases reaching minimum values and intermediate values of $V_{[Pb^{2+}]}$ 3.34 Åto 3.240 Å. After that ID diminishes until it reaches initial values.

The lattice constant (a) was calculated by using the equation for ZB system applied to the peaks in the sampled $2\theta$ interval a close agreement with the reported results in literature. PCJDS card No 80-0019. The XRD data were also used to estimate the grain size (GS) of the crystallites by Scherer's equation [36]

$$GS = \frac{k\lambda}{\beta \cos\theta} \qquad (10)$$

and the average value with its corresponding error was plotted against the $V_{[Pb^{2+}]}$ of CdS0-CdS:Pb-PbS0 samples (Fig. 8). The XRD data were Although this procedure is not suitable for determination of absolute lattice parameters with high accuracy, it allows the relative comparison of a values as all the samples have been analysed under the same experimental conditions. In the same Fig. 8 are reported the values of pure ZB CdS (JCPDS 10-454).

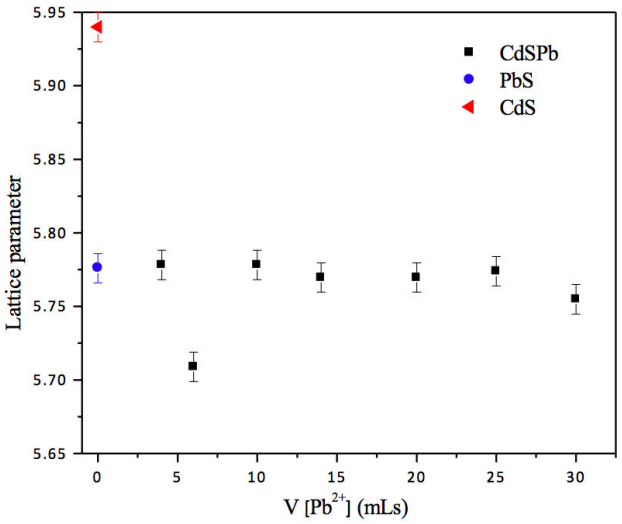


FIGURE 8. Lattice parameter (111) for Wurzite (WZ) and zinc blende phase (ZB), CdS0-CdSPb-PbS0 samples.

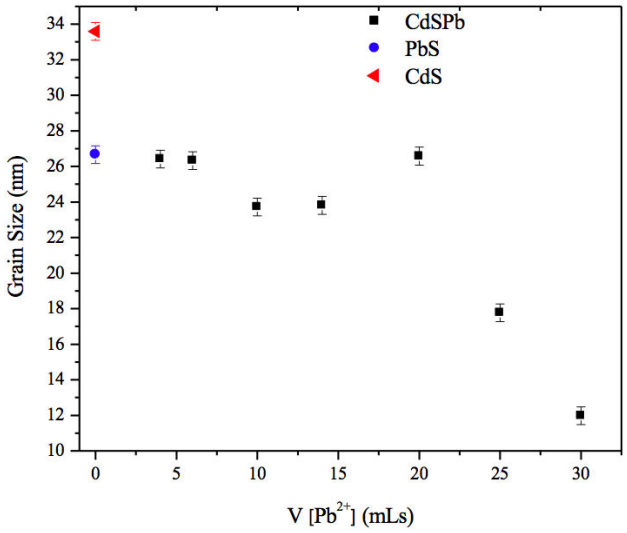


FIGURE 9. Grain size (GS), CdS0-CdSPb-PbS0 samples, calculated from XRD peak.

It can be seen that it decreases as $V_{[Pb^{2+}]}$ increases, suggesting the formation of a solid solution and it remains almost constant for higher $V_{[Pb^{2+}]}$. This is consistent with a singlephase material at lowest $V_{[Pb^{2+}]}$and a two-phase material at higher $V_{[Pb^{2+}]}$ Moreover, the lattice constant decreases with increasing $V_{[Pb^{2+}]}$ in the film which is an effect of $Pb^{2+}$ substituting $Cd^{2+}$ in CdS. A possible explication to this experimental fact can be given as follows: the ionic radii data are $Cd^{2+}$ = 0.95 Å, $S^{2-}$ = 1.84 Å, $Pb^{2+}$ =1.12 Å. The (111) ID of ZB phase in bulk are 0.3367 nm. These values are larger than the ID values found for the CdS0-CdSPb films in this work. We think it is probable that values of ID in CdS:Pb films are owing to the existence of $Cd^{2+}$ vacancies. For a relative low concentration of $Pb^{2+}$ ion, this can be, in a large majority, be situated in: [33,34] (a) $Cd^{2+}$ vacancies sites which otherwise would be empty, (b) in $Cd^{2+}$ sites provoking the appearing of $Cd^{2+}$ interstitial, and (c) in interstitial positions. For higher $V_{[Pb^{2+}]}$, the material behaves like a solid solution, the generation of $Cd^{2+}$ vacancies, whose creation is needed to charge balance, start to be important in number and given the relative ionic radius of $S^{2-}$, in CdSPb6 sample the shrinkage of the lattice occurs. There is a tendency of CdSPb14 to CdSPb30 to growth films probably due to all of the possible $Pb^{2+}$ species present in $Cd^{2+}$ sites and interstitials positions, and also to the existence of PbS, which distort the crystalline lattice and provoke disorder. The distortion produces a strong strain which affects the interatomic distances, this similar fact has already been reported [35]. In this work, the strain and distortion of the lattice can be smaller. The appearing of S2-ions into the material favours the relaxing of the lattice. A comparison of inter-planar spacing calculated from X-ray and electron diffraction patterns with the standard value shows were $\lambda$ is the wavelength of X-ray radiation (0.15406), k the Scherer's constant (k = 0.9), and $\theta$ the characteristic X-ray radiation and $\beta$ was the full-with-at-half-maximum of plane (in radians). The GS was plotted vs.

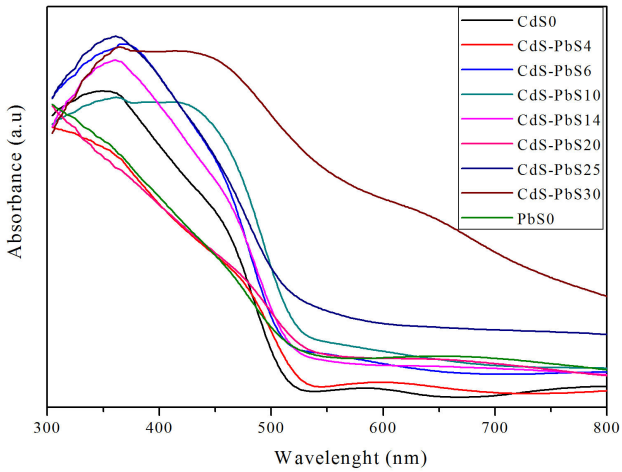


FIGURE 10. Optical absorbance spectra of the CdS0-CdSPb-PbS0 thin films.

$V_{[Pb^{2+}]}$ and displayed in Fig. 9. It can be seen that GS reduces ∼27 to 24 nm in interval $0 \leq V_{[Pb^{2+}]} \leq 14$ mLs, reaching a minimum ∼12 nm when $V_{[Pb^{2+}]}$ 30 mLs. These small-size nanostructures have large surface to volume ratio, which plays a dominant role in optical properties of the nanostructures.

Optical absorbance (A), transmittance (T) and spectra of CdS0-CdS:Pb-PbS0 thin films have been recorded in the 300-850 nm wavelength range. Thin films absorb heavily throughout the UV-Vis regions but moderately in the NIR region. Figure 10 shows that the absorption edge shifts towards larger wavelength for CdS:Pb thin films compared to as deposited CdS0 thin films. The characteristic absorption shoulder due to the CdS0 nanoparticles appear in the wavelength 350-450 nm range. At the absorption edge, only the larger particles contribute to A. In the smaller wavelength range, particles with smaller sizes contribute more and at region of A maximum, all particles contribute to A [37]. The shoulder

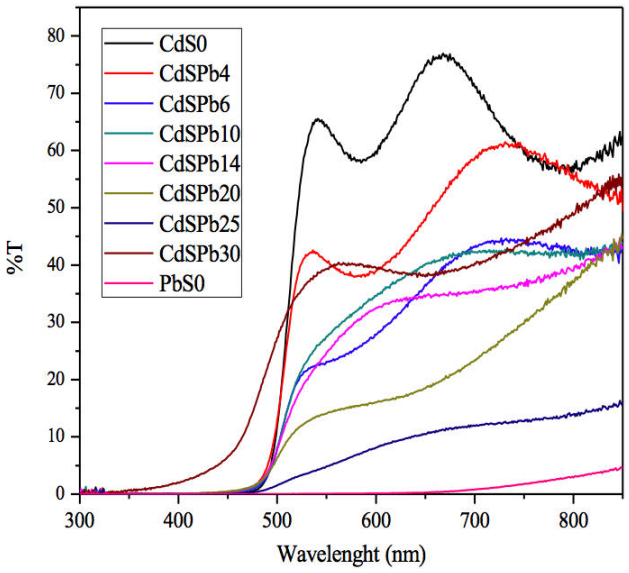


FIGURE 11. Optical transmittance spectra of the CdS-CdSPb-PbS thin films.

of CdSPb10 film at ∼450 nm position reflects the band gap ($E_g$) of the nanoparticles [38]. Compared to CdS0, the absorption spectra of CdS:Pb and PbS0 nanoparticles have significantly blue-shifted due to the reduction of the particles size. However, the absorption of the samples is highly blue-shifted from the bulk CdS0 (512 nm). This shifting is due to quantum confinement effect [39].

Figure 11 shows the optical T against wavelength for CdS0CdS:Pb-PbS0 layers. Usually the deposition parameters affect the optical properties of thin films. Interference fringes area can be seen in CdS0 film. The T spectra show a decrease and sharp fall in the transmission near the fundamental absorption when doping increases. In both CdSPb25 and CdSPb30 samples the whole trend is similar, namely the T decreases totally; however more decrement is observed in sample CdSPb30. The T spectra showed less transparency with CdS0 film. This may be attributed to more scattering of photons by the introduction of dopant as foreign $Pb^{2+}$ ions, which may reduce T. This decrease in T with $V_{[Pb^{2+}]}$ is expected, because increases the number of the charge carriers which increases the absorption in the film, and decreases the transmission of light. In a visual inspection, the samples appear homogeneous with a color changing from transparent yellow (CdS0) to transparent brownish CdS:Pb and PbS0 films according to Fig. 1. The CdS0 sample has a T ∼68 and 78% in the ∼520 and 700 nm range respectively.

The CdS:Pb samples have a T about ∼60 and 20% in the ∼520 and 700 nm range respectively. The high value of the transmittance is suitable for solar cell applications where CdS0 can be used as a window material in heterojunction solar cell such as the CdS/CdTe solar cell [40]. The T of the films for wavelength values smaller than the cut-off wavelength (∼510 nm) is a function of film thickness; and the T decreases as function of thickness. Absorption toward longer wavelength for thicker films was also observed. These observations are in agreement with Sahay [41]. The low transparency of the CdS0 sample might be due to loosely adhered colloids formed by homogeneous growth process and to the films thickness.

The absorption edge for T of CdSPb10-CdSPb20 films is approximately unaffected with $V_{[Pb^{2+}]}$. The change in T after the absorption edge is related to the uniformity of the CdS:Pb films showing an interference maxima and minima while the other ones does not show them. This means that the quality of the films had improved at the higher doping. T decreases totally; however more decrement is observed in the CdSPb25 and CdSPb30 samples. In a visual inspection, the samples appear homogeneous with a colour changing from yellow (CdS0) to transparent brownish (CdSPb30). On the other hand, as one sample is studied from the prospective of CdS:Pb samples, the pertinent T decreases. It is usually presumed that the T of the films decreases with GS in the visible region of spectrum due to light scattering on their rough surfaces.

From the T spectra we have calculated the optical band gaps ($E_g$) of the Cd0-CdS:Pb-PbS0 thin films. The absorption coefficient $\alpha$ and the incident photon energy $h\nu$ are related by the following equation [35]

$$\alpha h\nu = (E_g - h\nu)n$$

where A is constant, and the exponent $n$ depends on the type of transition and may have values 1/2, 2, 3/2 and 3 corresponding to allowed direct, allowed indirect forbidden and indirect transition respectively. The optical $E_g$ values were obtained by extrapolating the linear portion of the plots of $(\alpha h\nu)2$ vs. $h\nu$ to $\alpha = 0.43$ The plot of $(\alpha h\nu)2$ vs. $(h\nu)$ is shown in Fig. 12 which is linear at the absorption edge, indicating a direct allowed transition.

A study of CdS0 films revealed tensile strain along the WZ (002) plane, and dependence of strain on the GS is responsible for variation of $E_g$ with the film thickness [44]. It was found that the optical absorption edge shifted to higher wavelengths as the films thickness and electrical resistivity decrease for thicker films. This was attributed to an increase of crystalline size, the degree of preferred orientation, internal microstrain and stoichiometry on the film [45]. It can be seen that there is a difference in slope between in CdSPb4 and CdSPb30 in the 320-450 nm wavelength range. In a crystalline or polycrystalline material, direct or indirect optical transitions are possible depending on the structure of that material. It was suggested that the extended absorption-edge spectrum of a normal direct $E_g$ semiconductor, such as PbS, usually indicates the possibility of direct transition. This anomaly could be due to the difference in sample thickness which was ∼200-600 nm [46]. At any value of Pb concentration, the optical $E_g$ decreases; this fact can be attributed to improvement of crystallinity [24]. Also, during the doping, at the surface and at the grain boundaries, traps would be created within the $E_g$ that may cause formations of the states near the band edge and so lead to $E_g$ shrinkage. The apparent blue shift is also indicative of size quantization in

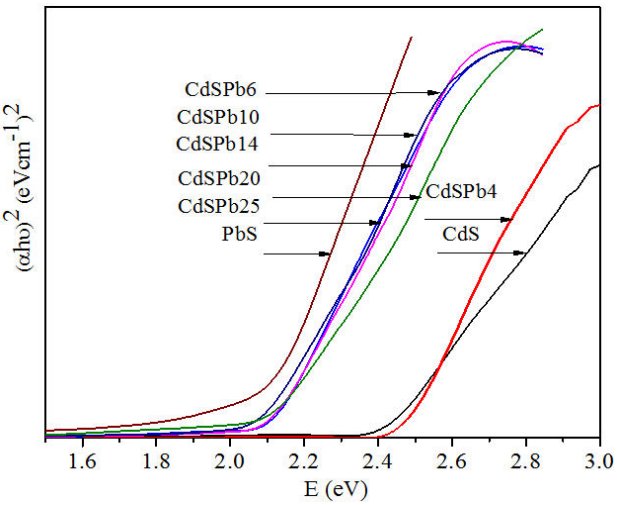


FIGURE 12. Band gap ($E_g$) values of the CdS0-CdSPb-PbS.

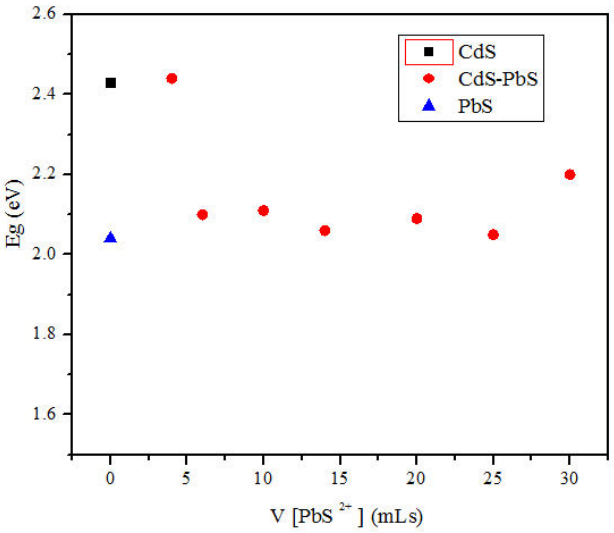


FIGURE 13. Band gap values of the CdS-CdSPb-PbS.

CdS:Pb-PbS0 nanoparticles. In our synthetic system, the investigations of CdS0-CdS:Pb-PbS0 formation indicated that the nucleation and growth were controlled. Firstly, $NH_3$, as a strongly monodentating solvent, was ready to form relatively stable $Cd^{2+}$ and $Pb^{2+}$ complexes. Next, the thiourea generates $S^{2-}$ ions slowly and homogeneously. The $S^{2-}$ ions react with the $Cd^{2+}$ ions that chelated with NH3 in a reversible and effective pathway to produce CdS:Pb nanoparticles. It is observed that the $E_g$ decreased with an increase in molar fraction, the reason for this may be attributed to decreases in thickness CdS:Pb films [47].

This fact clearly shows then that it enhances with Pb doping. In other words, this means extending tail states within the $E_g$ that leads to the $E_g$ narrowing. $E_g$ vs. $V_{[Pb^{2+}]}$ are showed in Fig. 13, the values are in 2.1-2.4 eV range. For the CdS0-CdS:Pb-PbS0 films, the incorporation of this doping agent, as well as a possible sulfur deficiency, will give rise to donator levels in the $E_g$ of CdS0. As the $V_{[Pb^{2+}]}$ increases, the donor levels become degenerate and merge with the conduction band of CdS:Pb, causing the conduction band to extend into the forbidden region which reduces the $E_g$ [48]. However, for PbS0, $E_g$ = 1.94 eV and $E_g$ = 3.14 eV are related to the $E_0$ and $E_1$ transitions respectively [49]. These data and the literature values are used for modeling of the optical constants of PbS over 0.4-5.5 eV photon energy range, including the $E_g$ ($E = 0.4$ eV) region. Calculated $E_g = 2.0$ eV $(\alpha h\nu)^2$ vs. $h\nu$ spectra are in satisfactory agreement with the experiment over the entire range of photon energies.

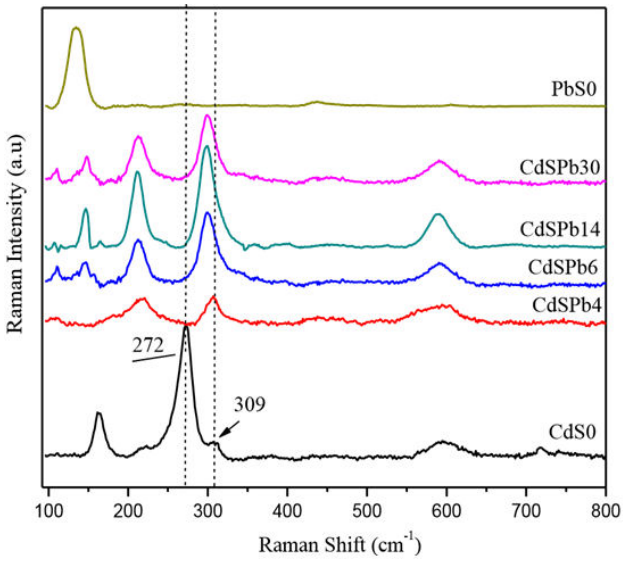


FIGURE 14. Raman spectroscopic on CdS0-CdSPb-PbS0 films.

Raman spectroscopy measurements on CdS0-CdS:Pb-PbS0 films (Fig. 14) were performed at temperature of 25°C. A CdS0 Raman spectrum shows two peaks corresponding to IL and 2LO at 207 and 600 $cm^{-1}$. The prominent peak CdS:Pb at 209 $cm^{-1}$ is attributed to either the ZB 1LO phonon or WZ A1(LO)/E1(LO) phonons. This Raman shift results from phase transition in thin CdS0-CdSPb films from ZB due to doping, which should be about 18% and causes the E1(TO) peak to shift from 240 $cm^{-1}$ (original position in WZ CdS) to 290 $cm^{-1}$. Since the observed peak for the annealed CdS films was at 276 $cm^{-1}$, they ruled out to TO phonon possibility and we can attributed this peak to a shift in the E1(TO) peak WZ CdS. The peaks associated with confined LO phonon modes, as well as their over tones (2LO), are clearly seen for all CdS:Pb samples. For both optical modes (LO and 2LO), characteristic broad shoulders contribute to lower frequency tails and their origin can be ascribed to both: (i) the effect of optical phonon confinement50 and (ii) the surface optical phonons of spherically shaped embedded in the effective dielectric medium of CdS0. Raman spectra for PbS0 contains bands at 140, 338, 425, 502, 590 $cm^{-1}$. The major bands are at 141, 287 $cm^{-1}$. The strong band centered at 140 $cm^{-1}$ originates from the combination of longitudinal and transverse acoustic phonon modes in PbS crystals [51]. The intense, narrow peak at ∼68 $cm^{-1}$ and the small peak at 45 $cm^{-1}$ are acoustic modes of PbS [52]. These

results are in good agreement with our XRD results and confirm the formation of CdS0 ZB structure and CdS:Pb W. In Fig. 14 we observe two main peaks located at ∼272 and 609 $cm^{-1}$ for CdS0 films which correspond to 1LO modes and 2LO modes of ZB-CdS, respectively. The spectra indicate the slightly shift LO mode towards high wavenumber side and the intensity increase of the Raman peaks by increasing $V_{[Pb^{2+}]}$. A decrease in intensity with GS is expected due to phonon confinement, the magnitude of shift is larger than the 1 $cm^{-1}$ reported for spherical CdS particles in the same range [53]. Peaks are observed corresponding to scattering from PbS0 phase, which confirm the doping of $Pb^{2+}$ ion in the host nanocrystals. Position of 1LO phonon peaks (∼309 $cm^{-1}$) deduced from Raman spectrum of CdS:Pb is shifted toward higher wave number side in comparison with the 1LO phonon peak position CdS (∼297 $cm^{-1}$) nanocrystals, which substantiates the formation of alloys nanocrystals. The peak intensity corresponding to ∼196 $cm^{-1}$ and ∼160 $cm^{-1}$ was found increasing with $V_{[Pb^{2+}]}$. So it is suggested that the band belong to transition from CdS0 to PbS0. One more feature observed in the presents results is a weak shoulder at slightly lower number (275 $cm^{-1}$) accompanying 1LO peak. Such shoulder in CdS films has been attributed to the presence of E1(TO) phonon mode. This mode is presented when the ZB and WZ structure are comparable in bulk of the microcrystalline. This means that the structure has a higher degree of disorder, and crystallites have many small regions of ZB-CdS0 coexisting with many small regions of WZ-CdS0 [54]. Thus for ZB structure, only one triply degenerate mode is Raman active. For the WZ-CdS0 structure the analysis result in 2A1+2B2+2E1+2E2 modes, out of one, A1 and E1 are acoustic modes; B1 is silent mode giving A1+E1+2E2 optical Raman-active modes. Thus, if the structure is WZ more number of modes is expected. The spectra indicate that the modes intensity decreases by increasing $V_{[Pb^{2+}]}$. A similar trend with increasing $Co^{2+}$ concentration in CdS growth by implantation has already been reported and explained as due to GS effect in the films [7]. The failure to observe differences between the CdS:Pb, CdS0 and PbS0 spectra could be due to one or several of a variety factors. The smallest diameter produced in this study is ∼15-24 nm. Additionally, the XRD results suggest that the nanoparticles produced and the nanocrystals consist of the string of crystallites whose average lengths are no much greater than their diameters, hence the apparent anisotropic effect of the samples may be far less than that suggested by the overall aspect ratio of nanoparticles. The shifting of these modes can be attributed to strain, stress effects, defects, phonon confinement, variation in phonon relaxation with GS and changes in the lattice parameters with GS [7]. PbS is a relatively weak Raman scatter at room temperature and susceptible to laser-induced degradation upon intense irradiation. Here, relatively higher power (25 mW) is applied to irradiate the CdS:Pb and PbS0 samples in order to investigate their stabilities toward laser irradiation rather that Raman spectrum of PbS0. The Raman spectra of the PbS0 sample, under irradiation, display a peak located at 155 nm with near absence of any peak, which suggest that it is the most stable [23]. According to earlier reports for PbS materials, Raman peaks at 210, 271, and 451 $cm^{-1}$ should be observed, corresponding to a one longitudinal optical phonon mode, a two-phonon process, and two longitudinal optical phonon mode, respectively [56,57]. It is well-known that in a crystalline semiconductor, the observed Raman shift usually correspond to the longitudinal optical phonons (LO), whereas other modes, such as the transverse optical phonons (TO) and the surface phonons (SP) are, in general, not observable because of symmetry restrictions and low intensities, respectively. However, as the surface-to-volume ratio is large for nanostructured materials, it is possible to observe the SP mode by Raman scattering measurements.

## 4. Conclusions

The effect of $V_{[Pb^{2+}]}$ on the morphological, crystal structure, optical band gap properties of thin films has been investigated. The composition study showed that these films were stoichiometric slight in sulphur deficiency. The XRD pattern revealed the films are crystalline with average grain size decreased with $V_{[Pb^{2+}]}$ increasing. These films displayed also large final thickness and their surface morphologies were composed of small grains with an approximate size of 27-12 nm. Optical absorbance measurements indicated the existence of direct transition with corresponding energy gap in a 2.1-2.4 eV range. These films also exhibited a good transmittance of about 60% in visible and near infrared regions of the electromagnetic spectrum, allowing their use as a window layer in high efficiency thin films solar cell. In summary, we have found an efficient process to introduce $Pb^{2+}$ ions into the CdS lattice with, practically, no large damage to the lattice.


1. B. T. Wilhelm and J. R. Landry, *RNASeq-quantitative measurement of expression through massively parallel RNA-sequencing. Methods* (San Diego, Calif.), **48** (2009) 249. H. Kanasawa, S. Adachi, *J. Appl. Phys.* **83** (1998) 5997.
2. N. Choundhury and B. K. Sharma, *Thin Solid Films*. **519** (2011) 2132.
3. J. J. Valenzuela, B. R Ramírez G. A. Mendoza and L. M. Sotelo, *Thin Solid Films.***441** (2003) 104.
4. S. Chandramohan, A. Kanjilal, S. Sarangi, N. S. Majumder, R. Sathamoorthy, and T. Som, *Appl. Phys. A* **99** (2010) 837.
5. H. Khallaf, C. Guangyu, O. Lupan, L. Chow, S. Park, and A. Schulte, *Appl. Surf. Sci*. **255** (2009) 4129.

6. H. M. Upadhyaya and S. Chandra, *J. Mat. Sci*. **29** (1994) 2734.
7. C. Z Zhang, W. C. Wei, and Y. H. Xiao, *Crystal Growth & Desing* **7** (2007) 580.
8. K. L. Narayanan, M. Yamaguchi, P. J. A. Dávila, M. R. Lozada, M. O. Portillo, and O. Zelaya á. *Vacuum* **81** (2007) 1430.
9. L. G. Sillen, and A. E. Martell, *Chem. Soc., London* **17** (1964) 8.
10. A. Yuchi, H. Wada, and G. Nakagawa, *Analy. Sci.***1** (1985) 19.
11. J. A. Dean, *Lange's Handbook of Chem*. 13th ed. (New York: McGraw-Hill. 1987). p. 5.
12. Q. Q. Liu, J. H. Shi, Z. Q. Li, D. W. Zhang, X. D. Li, Z. Sun, L.Y. Zhang, and S. M. Huang, *Physica B*. **405** (2010) 4360.
13. M. Froment, and D. Lincot, *Electrochem. Acta* **40** (1995) 1293.
14. M. R. Palomino, *et al*., *Nanotech.* **13** (2013) 1.
15. M. O. Portillo, *et al*., *Nanotechnology.* **1** (2012) 1.
16. Zhai, R. Wang, S. Xu, H. Wang, and H. Yan. *Mat. Lett.* **59** (2005) 1497.
17. D. Fan, H. Wang, Y. Zhang, J. Cheng, B. Wong, and H. Yan, *Mat. Chem. and Phys.* **80** (2003) 44.
18. C. D. Lokhande, *et al*., *Thin Solid Films.* **330** (1998) 70.
19. C. A. Carrillo, *et al*., *Mat. Lett.* **12** (2014) 19.
20. H. Moualkia, S. Hariech, and M. S. Ainda, *Thin Solid Films*. **518** (2009) 1259.
21. X. Guo, Y. Deng,. B. Tu, and D. Zhao, *Langmuir*. (2010) **26** 702.
22. S. Liu, S. Xiong, K. Bao, L. Cao, and Y. Quian, *J. Phys. Chem. C* **113** (2009) 13002.
23. Li. Chunguang, Y. Zhao, F. Li, Z. Shi, and S. Feng, *Chem. Mater. 22* (2010) 1901.
24. Y. Yu, S. K. Zhang, and J. Sun, *Molec. Struct*. **1031** (2013) 194.
25. Z. A. Abdolahzade, and F. E. Ghodsi, *J. Luminescence*. (2013) **141** 121.
26. K. Yamaguchi, T. T. Yoshida, and M. S. Hideki, *J. Phys. Chem. B* **102** (1998) 9677.
27. G. Murugadoss, *Superlattices and Microstructures*, **52** (2012) 126.
28. M. Guglielmi, A. Martucci, J. Fick, and G. Vitrant, *J. Sol-Gel Sci. Technol.* (1998) 229-240.
29. S. Natalia, R. A. A. Kozhenikova, F. Hergert, and A. Magery, *Thin Solid Films*. **517** (2000) 2586
30. J. A. Lange's, *Handbook of Chemistry*, (McGrawHill Book Co., Beijing, 1999).
31. B. R. Ortega and D. Lincot, *J. Electrochem. Soc.* **140** (1993) 3464.
32. I. Broser, H. Maier, and H. Schult, *J. Phys. Rev.* **140** (1965) 2135.
33. M. Grus, and A. Siroka, *Physica. B 266* (1999) 139.
34. M. O. Portillo *et al*., *Electrochem. Sci. Soc.* **153** (2006) 926.
35. M. Esmaili, A. Habibi-Y, and J. Chin, *Catal.* **32** (2011) 933.
36. C. S. Tiwary, R. Sarkar, P. Kumbhakar, and A. K. Mitra, *Phys. Lett. A* **372** (2008) 5825.
37. M. Maleki, G. M. Sasani, S. Mirdamadi, and R. Ghasemzadeh, *Phys. Quant. Electr. Optoelectr.* **10** (2007) 30.
38. R. K. Subba, B. Kumar, and J. Anil. *Mat, Sci. Electron.* **11** (2000) 269.
39. I. S. Jamil, and R. N. Ahmad-B, *J. Mater Res. Technol.* **2** (2013) 221.
40. P. P. Sahay, R. K. Nath, and S. Tewari, *Cryst. Res. Technol.* **42** (2007) 275.
41. I. Nascu, C. V. Pop, I. E. Indrea, and I. Bratu, *Thin Solid Films.* **307** (1997) 240.
42. S. Singhal, C. A. Kumar, and H. O. R. Gupta, *Chandra. Nanoscale Res. Lett.* **5** (2010) 323.
43. A. Cortes, H. Gómez, R. E. Marotti, G. Riveros, and E. A. Dalchiele, *Solar Ener. Mat, & Solar Cell.* **82** (2004) 21.
44. E. J. Pantoja, and X. Mathew, *Solar Ener. Mat. & Solar Cell.* **76** (2003) 313.
45. K. S. Ramaiah, R. Pilkington, D. A. E. Hill, R. D. Tomlinson, and A. K. Bhatnagar, *Mat. Chem. Phys.* **68** (2001) 22.
46. M. A. Barote, A. A. Yadav, L. P. Deshmukh, and E. U. Masumdar, *J. Non-Oxide Glass.* **2** (2010) 151.
47. H. Khallaf, G. Chai, L. C. O. Lupan S. Park, and A. Schulte, *J. Phys. D: Appl. Phys.* **41** (2008) 185304.
48. H. Kanazawa, and S. Adachi, *J. Appl. Phys.* **83** (11) (1998) 5997.
49. D. Routkevitch, T. Bigioni, M. Mokovits, and J. Ming Xu, *J. Phys. Chem.* **100** (2004) 14037.
50. N. E. S. Freitas, *et al*., *J. Raman Spectra.* **44** (2013) 1022.
51. G. D. Smith, S. Firth, R. J. H. Clark, and M. Cardona, *J. Appl. Phys.*, **92** (2002) 4375.
52. T. D. Krauss, and F. W. Wise, *Phys. Rev. 55* (1997) 9860.
53. D. Routkevitch, T. L. Halslett, L. Ryan, T. Bigioni, C. Douketis, and M. Moskovits, *Chem. Phys.* **210** (1996) 343.
54. N. Badera, *et al*., *Solar Ener. Mat. & Solar Cell.* **92** (2008) 1646.
55. T. D. Krauss, F. D. Wise, and D. B Taner, *Phys. Rev. Lett.* **76** (1996) 1376.